PHYSICAL REVIEW D **87,** 065027 (2013)

Relativistic lattice Boltzmann model with improved dissipation

M. Mendoza,[1,*] I. Karlin,[2,†] S. Succi,[3,‡] and H. J. Herrmann[1,4,§]

[1]*ETH Zürich, Computational Physics for Engineering Materials, Institute for Building Materials, Schafmattstrasse 6, HIF, CH-8093 Zürich, Switzerland*

[2]*Department of Mechanical and Process Engineering, ETH Zürich, Sonneggstrasse 3, ML K 20, CH-8092 Zürich, Switzerland*

[3]*Istituto per le Applicazioni del Calcolo C.N.R., Via dei Taurini, 19 00185 Rome, Italy and Freiburg Institute for Advanced Studies, Albertstrasse, 19, D-79104 Freiburg, Germany*

[4]*Departamento de Física, Universidade Federal do Ceará, Campus do Pici, 60455-760 Fortaleza, Ceará, Brazil*

(Received 16 January 2013; published 26 March 2013)

We develop a relativistic lattice Boltzmann (LB) model, providing a more accurate description of dissipative phenomena in relativistic hydrodynamics than previously available with existing LB schemes. The procedure applies to the ultrarelativistic regime, in which the kinetic energy (temperature) far exceeds the rest mass energy, although the extension to massive particles and/or low temperatures is conceptually straightforward. In order to improve the description of dissipative effects, the Maxwell-Jüttner distribution is expanded in a basis of orthonormal polynomials, so as to correctly recover the third-order moment of the distribution function. In addition, a time dilatation is also applied, in order to preserve the compatibility of the scheme with a Cartesian cubic lattice. To the purpose of comparing the present LB model with previous ones, the time transformation is also applied to a lattice model which recovers terms up to second order, namely up to the energy-momentum tensor. The approach is validated through quantitative comparison between the second- and third-order schemes with Boltzmann approach multiparton scattering (the solution of the full relativistic Boltzmann equation) for moderately high viscosity and velocities, and also with previous LB models in the literature. Excellent agreement with BAMPS and more accurate results than previous relativistic lattice Boltzmann models are reported.

DOI: 10.1103/PhysRevD.87.065027 PACS numbers: 47.11.−j, 12.38.Mh, 47.75.+f

I. INTRODUCTION

Relativistic hydrodynamics and kinetic theory play a major role in many forefronts of modern physics, from large-scale applications in astrophysics and cosmology, to microscale electron flows in graphene [1–3], all the way down to quark-gluon plasmas [4–6]. Because of their strong nonlinearity and, for the case of kinetic theory, high dimensionality as well, the corresponding equations are extremely challenging even for the most powerful numerical methods, let alone analytics. Recently, a promising approach, based on a minimal form of relativistic Boltzmann equation, whose dynamics takes place in a fully discrete phase-space and time lattice, known as the relativistic lattice Boltzmann (RLB), has been proposed by Mendoza *et al.* [7–9] (and subsequently revised in Ref. [10] for enhancing numerical stability). To date, the RLB has been applied to the simulation of weakly and moderately relativistic fluid dynamics, with Lorentz factors of $\gamma \sim 1.4$, where $\gamma = 1/\sqrt{1 - v^2/c^2}$, with c being the speed of light and v the speed of the fluid. This model correctly reproduces shock waves in quark-gluon plasmas, showing excellent agreement with the solution of the full Boltzmann equation as obtained by Bouras *et al.* using Boltzmann-approach multiparton scattering (BAMPS) [11,12]. The RLB makes use of two distribution functions, the first one modeling the conservation of number of particles, and the second one modeling the momentum-energy conservation equation. The model was constructed by matching the first- and second-order moments of the discrete velocity distribution function to those of the continuum equilibrium distribution of a relativistic gas. However, it was not able to reproduce the right velocity and pressure profiles for the Riemann problem in quark-gluon plasmas, for the case of large values of the ratio between the shear viscosity and entropy density, $\eta/s \sim 0.5$, at moderate fluid speeds ($v/c \sim 0.6$).

In order to set up a theoretical background for the lattice version of the relativistic Boltzmann equation, Romatschke *et al.* [13] developed a scheme for an ultrarelativistic gas based on the expansion on orthogonal polynomials of the Maxwell-Jüttner distribution [14] and, by following a Gauss-type quadrature procedure, the discrete version of the distribution and the weighting functions was calculated. This procedure was similar to the one used for the nonrelativistic lattice Boltzmann model [15,16]. This relativistic model showed very good agreement with theoretical data, although it was not compatible with a lattice, thereby requiring linear interpolation in the free-streaming step. This implies the loss of some key properties of the standard lattice Boltzmann method, such as negative numerical diffusion and exact streaming.

Very recently, Li *et al.* [17] noticed that the equation of conservation for the number of particles recovered by the

*mmendoza@ethz.ch
†karlin@lav.mavt.ethz.ch
‡succi@iac.cnr.it
§hjherrmann@ethz.ch

RLB model [7,8] exhibits spurious diffusive effects. They proposed an improved version of RLB, using a multi-relaxation-time collision operator in the Boltzmann equation, which allows independent tuning of the bulk and shear viscosities, yielding results for the Riemann problem closer to those of BAMPS [11] when the bulk viscosity is decreased. However, the third-order moment of the equilibrium distribution still does not match its continuum counterpart, and therefore the model still has problems in reproducing high $\eta/s \sim 0.5$ for moderately high velocities, $\beta = v/c = 0.6$. Thus, while surely providing an improvement on the original RLB model, the work [17] did not succeed in reproducing the vanishing bulk viscosity, which is pertinent to the ultrarelativistic gas, while the issue with the spurious diffusion remained unresolved.

Note that in the much more studied case of the lattice Boltzmann models for nonrelativistic fluids, the question of the choice of the lattice with higher-order symmetry requirements has only recently been solved, in the framework of the entropy-compliant constriction [18,19]. However, the lattices (space-filling discrete velocity sets) found in that case are tailored to reproduce the moments of the nonrelativistic Maxwell-Boltzmann distribution, and do not seem to be directly transferable to the present case of the relativistic (Maxwell-Jüttner) equilibrium distribution, which has fairly different symmetries as compared to the nonrelativistic Maxwell-Boltzmann distribution. Therefore, the extension of the previous LB models has to be considered anew.

In this paper, we develop a new lattice Boltzmann model capable of reproducing the third-order moment of the continuum equilibrium distribution, and still realizable on a cubic lattice. The model is based on a single distribution function and satisfies the conservation of both number of particles and momentum-energy equations. The model is based on the single-relaxation-time collision operator proposed by Anderson and Witting [14,20], which is more appropriate for the ultrarelativistic regime than the Marle model used in the previous works. Thus, the proposed model offers significant improvement on previous relativistic lattice Boltzmann models in two respects: (i) It captures the symmetry of the higher-order equilibrium moments sufficiently to reproduce the dissipative relativistic hydrodynamics at the level of the Grad approximation to the relativistic Boltzmann equation. (ii) It represents a genuine lattice Boltzmann discretization of space and time, with no need of any interpolation scheme, thereby avoiding the otherwise ubiquitous spurious dissipation. The new lattice Boltzmann model is shown to reproduce with very good accuracy the results of the shock waves in quark-gluon plasmas, for moderately high velocities and high ratios η/s.

The paper is organized as follows: in Sec. II, we describe in detail the model and the way it is constructed; in Sec. III, we implement simulations of the Riemann problem in order to validate our model and compare it with BAMPS and previous relativistic lattice Boltzmann models; and finally, in Sec. IV, we discuss the results and future work.

II. MODEL DESCRIPTION

A. Symmetries of the relativistic Boltzmann equation

To build our model, we start from the relativistic Boltzmann equation for the probability distribution function f:

$$p^\mu \partial_\mu f = -\frac{p_\mu U^\mu}{c^2 \tau}(f - f^{\mathrm{eq}}), \tag{1}$$

where the local equilibrium is given by the Maxwell-Jüttner equilibrium distribution [14],

$$f^{\mathrm{eq}} = A \exp(-p^\mu U_\mu / k_B T). \tag{2}$$

In the above, A is a normalization constant, c the speed of light, and k_B the Boltzmann constant. The 4-momentum vectors are denoted by $p^\mu = (E/c, \vec{p})$, and the macroscopic 4-velocity by $U^\mu = (c, \vec{u})\gamma(u)$, with $\vec{u}$ the three-dimensional velocity of the fluid. Note that we have used the Anderson-Witting collision operator [20] [rhs of Eq. (1)], making our model compatible with the ultrarelativistic regime. Hereafter, we will use natural units, $c = k_B = 1$, and work in the ultrarelativistic regime, $\xi \equiv mc^2/k_B T \ll 1$.

According to a standard procedure [13,15,16], we first expand the Maxwell-Jüttner distribution in the rest frame, $f^{\mathrm{eq}} = A \exp(-p^0/T)$, in an orthogonal basis. Since in the ultrarelativistic regime $p^0/T = \sqrt{\vec{p}^2/T^2 + m^2/T^2} \simeq p/T$, being $p = \sqrt{\vec{p}^2}$, we can write the equilibrium distribution in spherical coordinates:

$$\int g e^{-p_0/T} \frac{d^3 p}{p^0} = \int_0^\infty \int_0^\pi \int_0^{2\pi} g p e^{-p/T} dp \sin(\theta) d\theta d\phi, \tag{3}$$

where g is an arbitrary function of momentum. Following Romatschke [13], we can expand the distribution in each coordinate separately; and subsequently, by using a Gauss quadrature, we can calculate the discrete values of the 4-momentum vectors. Thus, the discrete equilibrium distribution can be written as

$$f_l^{\mathrm{eq}} = \sum_{i,j,k} a_{ijk}(U^\mu) P_i(\theta_l) \mathcal{R}_j(p_l) F_k(\phi_l), \tag{4}$$

where the coefficients $a_{ijk}(U^\mu)$ are the projections of the distribution on the polynomials $P_i(\theta_l)\mathcal{R}_j(p_l)F_k(\phi_l)$, and the discrete 4-momenta are denoted by $p_l^\mu = (p_l, p_l \cos(\phi_l)\sin(\theta_l), p_l \sin(\phi_l)\sin(\theta_l), p_l \cos(\theta_l))$. Consequently, the discrete form of the Boltzmann equation takes the form

$$f_l(x^\mu + p_l^\mu/p_l^0\delta t, t+\delta t) - f_l(x^\mu, t) = -\frac{p_{l\mu}U^\mu \delta t}{\tau p_l^0}(f_l - f_l^{\rm eq}). \quad (5)$$

However, note that in the streaming process on the right-hand side of Eq. (5), the distribution moves at velocity p_l^μ/p_l^0, which implies that the information travels (in a single time step) from each cell center to a position that belongs to the surface of a sphere of radius $c\ \delta t = 1$. Furthermore, to represent correctly the third-order moment of the equilibrium distribution,

$$P^{\alpha\beta\lambda} = \sum_l f_l^{\rm eq} p_l^\alpha p_l^\beta p_l^\lambda, \quad (6)$$

the number of points needed on the surface of the unit sphere exceeds 6 and 12, which correspond to the first neighbors for cubic and hexagonal closed packed lattices, respectively. This implies that, in general, the 4-vectors p^μ/p^0 cannot be embedded into a regular lattice, and therefore, an interpolation algorithm has to be used. By doing this, we are losing one of the most important features of lattice Boltzmann models, which is the exact streaming. Thus, within this spherical coordinate representation, the streaming process cannot take place on a regular lattice.

B. Moment projection of the equilibrium

In this work, we shall use a different approach to the quadrature representation. We first calculate a basis of orthonormal polynomials in Cartesian coordinates, unlike the spherical coordinate system used in Ref. [13], using as the equilibrium distribution at rest $w(p^0) = f^{\rm eq}(\vec{u} = 0)$ as a weight function. Once the polynomials are obtained, they are used to perform the expansion of the complete equilibrium distribution $f^{\rm eq}$. This procedure avoids extra terms in the product, $P_i(\theta_l)\mathcal{R}_j(p_l)F_k(\phi_l)$ for the discrete spherical case, which are not necessary if we only need to recover correctly the first three moments of the equilibrium distribution, simplifying considerably its expanded form.

In order to find the orthonormal polynomials, we first build the set

$$\mathcal{L}_j = \{1, p^0, p^x, p^y, p^z\}, \quad (7)$$

where the subindex $j = 1, 5$ explicitly denotes each element on the right-hand side. By calculating all possible combinations of the elements of $\mathcal{L}_k$ up to third order, we get the family of polynomials defined by

$$\mathcal{J}_k = \bigcup_{i,j,l=0}^{4} \{\mathcal{L}_i\mathcal{L}_j\mathcal{L}_l\}, \quad (8)$$

with k denoting each of the 35 elements of the set (there are only 35 nonrepeated elements out of the total 125). By performing a Gram-Schmidt orthogonalization with the inner product

TABLE I. Polynomials J_k, orthonormal with the weight function $w(p^0)$, in Cartesian coordinates (x, y, z).

Order	Polynomial J_k	k
0th	1	0
1st	$\frac{p^0-2}{\sqrt{2}}, \frac{p^x}{\sqrt{2}}, \frac{p^y}{\sqrt{2}}, \frac{p^z}{\sqrt{2}}$	1, 2, 3, 4
2nd	$\frac{(p^0-6)p^0+6}{2\sqrt{3}}, \frac{(p^0-4)p^x}{2\sqrt{2}}, \frac{(p^0-4)p^y}{2\sqrt{2}}$	5, 6, 7
	$\frac{(p^0-4)p^z}{2\sqrt{2}}, \frac{-(p^0)^2+(p^x)^2+2(p^y)^2}{4\sqrt{2}}, \frac{3(p^x)^2-(p^0)^2}{4\sqrt{6}}$	8, 9, 10
	$\frac{p^xp^z}{2\sqrt{2}}, \frac{p^yp^z}{2\sqrt{2}}, \frac{p^xp^y}{2\sqrt{2}}$	11, 12, 13
3rd	$\frac{1}{12}(p^0-6)^2p^0 - 2, \frac{((p^0-10)p^0+20)p^x}{4\sqrt{5}}$	14, 15
	$-\frac{(p^0-6)((p^0)^2-3(p^x)^2)}{24}, \frac{5(p^x)^3-3(p^0)^2p^x}{24\sqrt{5}}$	16, 17
	$\frac{((p^0-10)p^0+20)p^y}{4\sqrt{5}}, \frac{(p^0-6)p^xp^y}{4\sqrt{3}}, \frac{p^xp^yp^z}{4\sqrt{3}}$	18, 19, 20
	$\frac{(p^0-6)((p^x)^2+2(p^y)^2-(p^0)^2)}{8\sqrt{3}}$	21
	$\frac{p^x((p^x)^2+2(p^y)^2-(p^0)^2)}{8\sqrt{3}}$	22
	$\frac{p^y(-3(p^0)^2+3(p^x)^2+4(p^y)^2)}{24\sqrt{2}}, \frac{((p^0-10)p^0+20)p^z}{4\sqrt{5}}$	23, 24
	$\frac{(p^0-6)p^xp^z}{4\sqrt{3}}, -\frac{p^z((p^0)^2-5(p^x)^2)}{8\sqrt{30}}, \frac{(p^0-6)p^yp^z}{4\sqrt{3}}$	25, 26, 27
	$\frac{(p^0-6)p^yp^z}{4\sqrt{3}}, \frac{p^z(-(p^0)^2+(p^x)^2+4(p^y)^2)}{24\sqrt{2}}$	28, 29

$$\langle \mathcal{J}_r, \mathcal{J}_l\rangle = \int w(p^0)\mathcal{J}_r\mathcal{J}_l\frac{d^3p}{p^0}, \quad (9)$$

we construct the orthogonal polynomials,

$$J_k' = \mathcal{J}_k - \sum_{l=0}^{k-1}\frac{\langle \mathcal{J}_l, \mathcal{J}_k\rangle}{\langle \mathcal{J}_l, \mathcal{J}_l\rangle}\mathcal{J}_l, \quad (10)$$

and finally obtain the orthonormal ones as follows:

$$J_k = \frac{J_k'}{\sqrt{\langle J_k', J_k'\rangle}}. \quad (11)$$

The polynomials J_k, where the index k runs from 0 to 29 (there are only 30 linearly independent polynomials out of 35), are reorganized in ascending order and shown explicitly in Table I. Note that in this table, the 4-momentum has the notation $p^\mu = (p^0, p^x, p^y, p^z)$. Since these polynomials are orthonormal, there are no normalization factors, and the Maxwell-Jüttner distribution can be approximated up to third order in the momentum space by the following compact expansion:

$$f^{\rm eq} \simeq \sum_{k=0}^{29} w(p^0)a_k(T, U^\mu)J_k(p^\mu), \quad (12)$$

where the projections a_k are calculated by

$$a_k = \int f^{\rm eq}J_k(p^\mu)\frac{d^3p}{p^0}. \quad (13)$$

Since the Anderson-Witting model is only compatible with the Landau-Lifshitz decomposition [14,20], we must

calculate the energy density of the fluid by solving the eigenvalue problem

$$T^{\alpha\beta}U_\beta = \epsilon U^\alpha, \tag{14}$$

where ϵ is the energy density of the fluid, and

$$T^{\alpha\beta} = \int f p^\alpha p^\beta \frac{d^3p}{p^0} \tag{15}$$

is the momentum-energy tensor. For the particle density, we use the relation

$$n = U_\alpha \int f p^\alpha \frac{d^3p}{p^0}, \tag{16}$$

and by using the equation of state, $\epsilon = 3nT$, we can calculate the temperature of the fluid.

C. Discrete-velocity representation of the quadratures

Note that the above derivation using Cartesian coordinates still refers to the continuous 4-momenta. In order to discretize the above moment projection of the equilibrium distribution, we must choose a set of discrete 4-momentum vectors that satisfies the same orthonormality condition, namely

$$\int w(p^0)J_l(p^\mu)J_k(p^\mu)\frac{d^3p}{p^0} = \sum_i w_i J_l(p_i^\mu)J_k(p_i^\mu) = \delta_{lk}, \tag{17}$$

while at the same time, p^μ/p^0 corresponds to lattice points. Here, we choose to work with a cubic lattice, although the procedure described here also applies to other ones, e.g., the hexagonal closed packed lattice.

Since, due to its nature, p^μ/p^0 leads to velocity vectors which belong to a sphere of radius c in the space components, using the procedure in Ref. [13] will generally result in off-site lattice points. For this reason, we opt for another quadrature based on this orthonormality condition, and impose that the distribution function at rest frame should satisfy the moments of the equilibrium distribution up to sixth order. This is made to ensure that the fifth-order moment of the equilibrium distribution is recovered (at least at very low fluid velocities), which, in the context of the Grad theory for the Anderson-Witting model [14], is a requirement for the correct calculation of the transport coefficients, namely the shear and bulk viscosities and thermal conductivity. The condition for the sixth-order moment is to choose from the multiple lattice solutions the one that presents the highest symmetry to model the Maxwell-Jüttner distribution. In order to use general features of classical lattice Boltzmann models, like bounce-back boundary conditions to impose zero velocity on solid walls, we will also require that the weights w_i corresponding to the discrete 4-momentum vectors p_i^k have the same values as the ones corresponding to $-p_i^k$ (latin indices run over spatial components).

In order to generate on-site lattice points, we first divide the relativistic Boltzmann equation, Eq. (1), by p^0, to obtain

$$\partial_t f + v^a \partial_a f = -\frac{p_\mu U^\mu}{\tau p^0}(f - f^{\mathrm{eq}}), \tag{18}$$

where $v^a = p^a/p^0$ are the components of the microscopic velocity. In the ultrarelativistic regime, these microscopic velocities have all the same magnitude but, in general, different directions. In other words, the relativistic Boltzmann equation can be cast into a form where the time derivative and the propagation term become the same as in the nonrelativistic case, at the price of an additional dependence on p^0 in the relaxation term. However, since this newly acquired dependence remains local, we shall be able to find a discrete-velocity quadrature which also allows for a lattice Boltzmann-type discretization in time and space without any interpolation. Indeed, in a cubic cell of length $\delta x = 1$ there are only six neighbors, which are not sufficient to satisfy the orthogonality conditions and the third-order moment of the equilibrium distribution. However, by multiplying this equation by a constant R on both sides, and performing a time transformation (dilatation), $\delta t \to R\delta t'$ and $\tau \to R\tau'$, we obtain

$$\partial_{t'} f + \vartheta^a \partial_a f = -\frac{p_\mu U^\mu}{\tau' p^0}(f - f^{\mathrm{eq}}), \tag{19}$$

where we have defined $\vartheta^a = Rv^a$. Because of this transformation, the 4-momentum vectors are reconstructed through the relation

$$p^\mu = p^0(1, \vec{\vartheta}/R). \tag{20}$$

At this stage, we can choose the radius of the sphere such that the lattice points that belong to the surface of the sphere and the cubic lattice exhibit enough symmetries to satisfy both conditions. This is equivalent to solving the Diophantine equation,

$$n_x^2 + n_y^2 + n_z^2 = R^2, \tag{21}$$

where n_x, n_y, and n_z are integer numbers, being $\vec{\vartheta} = (n_x, n_y, n_z)$. Thus, we can determine the components of the discrete version of the velocities $\vec{\vartheta}$ which are needed for the streaming term in the Boltzmann equation, on the lhs of Eq. (19). However, on the rhs of this equation, and for the calculation of the discrete 4-momentum vectors via Eq. (20), we also need to know the discrete values of p^0. The 4-vector p^μ is needed to compute the orthonormality conditions given by Eq. (17) and the moments of the equilibrium distribution.

Because of the fact that p^0 is the magnitude of the 4-momentum, $p^0 = \sqrt{p^\mu p_\mu}$, in $(3+1)$-dimensional spacetime, it is natural to assume that its discrete values

can be calculated by using the weight function in spherical coordinates, $w(p^0) = 4\pi A (p^0)^2 \exp(-p^0)$, where the angular components have been integrated out, and using the zeros of its respective orthonormal polynomial of fourth order. (This is because we are interested in an expansion up to third order, so we need one more order to calculate the zeros.) This fourth-order polynomial is given by

$$\mathcal{R}^{(4)}(p^0) = \frac{1}{24\sqrt{5}}[120 + p^0(-240 + p^0[120 + (p^0 - 20)p^0])]. \quad (22)$$

To summarize, in order to calculate the discrete p_i^μ and their respective w_i, we first fix R and solve the equations

$$n_x^2 + n_y^2 + n_z^2 = R^2, \quad (23a)$$

$$\mathcal{R}^{(4)}(p^0) = 0 \quad (23b)$$

to obtain the solutions for n_x, n_y, n_z, and p. With these values, we build the discrete 4-vectors

$$p_{lm}^\mu = p_l^0(1, n_{x,m}/R, n_{y,m}/R, n_{z,m}/R), \quad (24)$$

where $l = 1, \ldots, 4$ denotes the four zeros of the polynomial $\mathcal{R}^{(4)}(p)$, and $m = 0, \ldots, \mathcal{M}$ denotes the triplets $(n_x, n_y, n_z)_m$ that satisfy the Diophantine equation, assuming that $\mathcal{M}$ is the number of solutions. Here, for simplicity, we regroup the pair of indexes $_{lm}$ to $_i$, so that we can label the discrete 4-momentums as p_i^μ, where $i = 1, \ldots, \mathcal{N}$ with $\mathcal{N} = 4 \times \mathcal{M}$.

Next, we replace these values into the equations

$$\int w(p^0) J_l(p^\mu) J_k(p^\mu) \frac{d^3p}{p^0} = \sum_i^{\mathcal{N}} w_i J_l(p_i^\mu) J_k(p_i^\mu) = \delta_{lk}, \quad (25a)$$

$$\int w(p^0) p^\mu p^\nu p^\sigma p^\lambda \frac{d^3p}{p^0} = \sum_i^{\mathcal{N}} w_i p_i^\mu p_i^\nu p_i^\sigma p_i^\lambda, \quad (25b)$$

$$\int w(p^0) p^\mu p^\nu p^\sigma p^\lambda p^\gamma \frac{d^3p}{p^0} = \sum_i^{\mathcal{N}} w_i p_i^\mu p_i^\nu p_i^\sigma p_i^\lambda p_i^\gamma, \quad (25c)$$

$$\int w(p^0) p^\mu p^\nu p^\sigma p^\lambda p^\gamma p^\beta \frac{d^3p}{p^0} = \sum_i^{\mathcal{N}} w_i p_i^\mu p_i^\nu p_i^\sigma p_i^\lambda p_i^\gamma p_i^\beta, \quad (25d)$$

$$w_i = w_j \quad (\text{if } p_i^k = -p_j^k), \quad (25e)$$

$$w_i \geq 0 \quad (25f)$$

and look for any solution for w_i that fulfills the above relations. Should none be found, we repeat the procedure with a different value of R. By performing this iteration process, we found that $R = \sqrt{41}$ is sufficient to recover up to the third-order moment of the Maxwell-Jüttner distribution, and up to the sixth order of this distribution in the Lorentz rest frame.

The corresponding discrete velocity vectors $\vec{\vartheta}_m$ are $(\pm 6, \pm 2, \pm 1)$, $(\pm 6, \pm 1, \pm 2)$, $(\pm 2, \pm 6, \pm 1)$, $(\pm 1, \pm 6, \pm 2)$, $(\pm 1, \pm 2, \pm 6)$, $(\pm 2, \pm 1, \pm 6)$, $(\pm 5, 0, \pm 4)$, $(\pm 5, \pm 4, 0)$, $(0, \pm 5, \pm 4)$, $(\pm 4, \pm 5, 0)$, $(0, \pm 4, \pm 5)$, $(\pm 4, 0, \pm 5)$, $(\pm 4, \pm 3, \pm 4)$, $(\pm 3, \pm 4, \pm 4)$, and $(\pm 4, \pm 4, \pm 3)$; with the values $p_l^0 \simeq 0.743$, 2.572, 5.731, and 10.95. Consequently, this gives a total of 4-momentum vectors $\mathcal{N} = 384$. However, the last condition in Eq. (25) allows some weights to become zero. Therefore, in our iteration procedure, we have taken the minimal number of 4-momentum vectors p_i^μ by requiring the maximum number of w_i to be zero. For this reason, there are only 128 vectors p_i^μ needed to fulfill the conditions in Eq. (25). In principle, all the velocity vectors $\vec{\vartheta}_m$ are needed, but only some of the combinations with p_l^0 are required. The detailed list of $\vec{\vartheta}_m$, p_l^0, and p_i^μ, and their respective discrete weight functions w_i are given in the Supplemental Material [21].

In Fig. 1, we report the configuration of the velocity vectors $\vec{\vartheta}$ to achieve the third-order moment of the Maxwell-Jüttner distribution function. The points correspond to lattice nodes of a cubic lattice that, at the same time, belong to the surface of the respective sphere of radius $R = \sqrt{41}$. The relatively large number of discrete velocities should not come as a surprise; in the case of nonrelativistic lattice Boltzmann, the number of discrete velocities also becomes high (at least 41 for achieving complete Galilean invariance in the nonthermal case and 125 in the thermal case; see Refs. [18,19]). Note that the specified values of p^0 play the same role in defining the

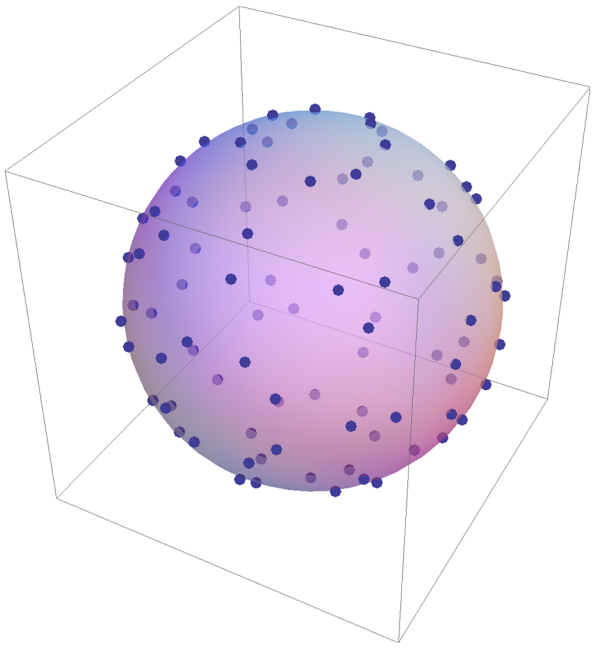

FIG. 1 (color online). Directions of the velocity vectors $\vec{\vartheta}_i$ to recover up to the third-order moment of the Maxwell-Jüttner distribution. The radius of the sphere is $R = \sqrt{41}$. The points represent lattice sites belonging to the sphere surface.

quadrature as the reference temperature (energy) in the nonrelativistic case [18,19].

Finally, we can write the discrete version of the equilibrium distribution up to third order,

$$f_i^{\mathrm{eq}} = w_i \sum_{n=0}^{29} a_n(T, U^\mu) J_n(p_i^\mu), \tag{26}$$

which is shown in detail in Eq. (B2) of Appendix B. Note that this distribution function recovers the first three moments of the Maxwell-Jüttner distribution in the ultrarelativistic regime:

$$\int f^{\mathrm{eq}} p^\mu \frac{d^3p}{p^0} = \sum_{i=1}^{128} f_i^{\mathrm{eq}} p_i^\mu = N_E^\mu, \tag{27}$$

$$\int f^{\mathrm{eq}} p^\mu p^\nu \frac{d^3p}{p^0} = \sum_{i=1}^{128} f_i^{\mathrm{eq}} p_i^\mu p_i^\nu = T_E^{\mu\nu}, \tag{28}$$

$$\int f^{\mathrm{eq}} p^\mu p^\nu p^\lambda \frac{d^3p}{p^0} = \sum_{i=1}^{128} f_i^{\mathrm{eq}} p_i^\mu p_i^\nu p^\lambda = P_E^{\mu\nu\lambda}, \tag{29}$$

where

$$N_E^\nu = nU^\nu \tag{30}$$

and

$$T_E^{\nu\mu} = -nT\eta^{\nu\mu} + 4nTU^\nu U^\mu, \tag{31}$$

being the number of particles 4-flow and the energy-momentum tensor, respectively, and

$$P_E^{\nu\mu\lambda} = -4nT^2(\eta^{\nu\mu}U^\lambda + \eta^{\nu\lambda}U^\mu + \eta^{\mu\lambda}U^\nu) + 24nT^2U^\nu U^\mu U^\lambda, \tag{32}$$

with $n = 2T^3$, and $\eta^{\mu\nu}$ the Minkowski spacetime metric tensor. However, the extension to the case of massive particles is straightforward by changing the coefficients a_n in Eqs. (13) and (26). Here, the subscript E denotes macroscopic quantities calculated with the equilibrium distribution.

D. Discrete relativistic Boltzmann equation

The Landau-Lifshitz decomposition [14] implies fulfillment of the following relations:

$$U_\mu N^\mu = U_\mu \int f p^\mu \frac{d^3p}{p^0} = U_\mu N_E^\mu = \int f^{\mathrm{eq}} p^\mu \frac{d^3p}{p^0}, \tag{33a}$$

$$U_\mu T^{\mu\nu} = U_\mu \int f p^\mu p^\nu \frac{d^3p}{p^0} = U_\mu T_E^{\mu\nu} = \int f^{\mathrm{eq}} p^\mu p^\nu \frac{d^3p}{p^0}, \tag{33b}$$

also called matching or fitting conditions, which are needed to obtain, upon integrating Eq. (1) in momentum space, the conservation of the number of particles 4-flow:

$$\partial_\mu N^\mu = 0, \tag{34}$$

and, multiplying by p^ν and integrating, the conservation of the momentum-energy tensor:

$$\partial_\mu T^{\mu\nu} = 0. \tag{35}$$

In order to calculate the transport coefficients, we need the third-order moment, so that upon multiplying Eq. (1) by $p^\nu p^\beta$ and integrating, we obtain

$$\partial_\mu P^{\mu\nu\beta} = -\frac{1}{\tau}(U_\mu P^{\mu\nu\beta} - U_\mu P_E^{\mu\nu\beta}). \tag{36}$$

Note that the lhs of this equation depends on the nonequilibrium third-order moment. However, by performing the Chapman-Enskog expansion [14] and reorganizing the terms, we can approximate Eq. (36) as

$$U_\mu P^{\mu\nu\beta} - U_\mu P_E^{\mu\nu\beta} = -\tau\partial_\mu P_E^{\mu\nu\beta}, \tag{37}$$

so that we need at least the third-order moment of the equilibrium distribution, $P_E^{\mu\nu\beta}$, to compute the dissipation coefficients (namely, bulk and shear viscosities and heat conductivity). This requirement is fulfilled in our discrete and continuum expansions of the equilibrium distribution via Eqs. (27)–(29). However, to recover full dissipation, we would also need to recover the first three moments of the nonequilibrium distribution, which according to the 14-moment Grad's theory, can be written as

$$N^\mu = (1-a)N_E^\mu + b_\alpha T_E^{\mu\alpha} + d_{\alpha\lambda}P_E^{\mu\alpha\lambda}, \tag{38a}$$

$$T^{\mu\nu} = (1-a)T_E^{\mu\nu} + b_\alpha P_E^{\mu\nu\alpha} + d_{\alpha\lambda}P_E^{\mu\nu\alpha\lambda}, \tag{38b}$$

$$P^{\mu\nu\beta} = (1-a)P_E^{\mu\nu\beta} + b_\alpha P_E^{\mu\nu\beta\alpha} + d_{\alpha\lambda}P_E^{\mu\nu\beta\alpha\lambda}, \tag{38c}$$

where a, b_α, and $d_{\alpha\lambda}$ are coefficients that carry the information on the transport coefficients [14]. Note that we need to recover terms up to the fifth order of the equilibrium distribution. In principle, this could be done by the procedure described on this paper, but the resulting value for R could be unpractically large. Nevertheless, at low velocities, $U^\mu \sim (1, 0, 0, 0)$, the Maxwell-Jüttner distribution can be approximated by the weight function $w(p^0)$, and in analogy to the discrete case, by w_i, and the fourth and fifth orders are recovered via Eq. (25). As a result, at relatively low velocities, we expect the nonequilibrium third-order tensor also to be fulfilled. Therefore, the transport coefficients for an ultrarelativistic gas, i.e., $\mu = 0$ for the bulk viscosity, $\eta = (2/3)P\tau$ for the shear viscosity, and $\lambda = (4/5T)P\tau$ for the thermal conductivity, also apply to our model.

To discretize the relativistic Boltzmann equation, we first implement the time transformation described in the previous section and integrate in time Eq. (1) between t' and $t' + \delta t'$. This yields

$$f(x^a + \vartheta^a \delta t', t' + \delta t') - f(x^a, t') = -\frac{p^\mu U_\mu}{\tau' p^0}(f - f^{\mathrm{eq}})\delta t'. \quad (39)$$

By changing $p^\mu \rightarrow p_i^\mu$, $f \rightarrow f_i$, and $\vartheta^a \rightarrow \vartheta_i^a$, we obtain

$$f_i(x^a + \vartheta_i^a \delta t', t' + \delta t') - f_i(x^a, t') = -\frac{p_i^\mu U_\mu}{\tau' p_i^0}(f_i - f_i^{\mathrm{eq}})\delta t'. \quad (40)$$

This relativistic lattice Boltzmann equation presents an exact streaming on the left-hand side, and the collision operator at the right-hand side looks exactly like its continuum version. Therefore, the conservation laws for the number of particles density 4-flow and the momentum-energy tensor are also fulfilled, as long as they are obtained by using the Landau-Lifshitz decomposition. This means that first, we need to calculate the momentum-energy tensor,

$$T^{\alpha\beta} = \sum_{i=1}^{128} f_i p_i^\alpha p_i^\beta, \quad (41)$$

and with this tensor, we solve the eigenvalue problem,

$$T^{\alpha\beta} U_\beta = T_E^{\alpha\beta} U_\beta = \epsilon U^\alpha, \quad (42)$$

obtaining the energy density ϵ and the 4-vectors U^α. Subsequently, the particle density can be calculated by

$$n = U_\mu N_E^\mu = U_\mu N^\mu = \sum_{i=1}^{128} f_i p_i^\mu U_\mu. \quad (43)$$

The temperature T is obtained by using the equation of state for the ultrarelativistic gas, $\epsilon = 3nT$. The transport coefficients are the same as in the continuum case, with the lattice correction resulting from second-order Taylor expansion of the streaming term. All factored in, the coefficients take the following expression: $\mu = 0$, $\eta = (2/3)P(\tau' - \delta t'/2)$, and $\lambda = (4/5T)P(\tau' - \delta t'/2)$. Note that by reverting the time transformation, we can write the transport coefficients as $\eta = (2/3)P(\tau - \delta t/2)/R$ and $\lambda = (4/5T)P(\tau - \delta t/2)/R$.

Summarizing, the present model does not present spurious dissipation in the number of particle conservation equation, in contrast to previous RLB schemes [7,8,10], and it also improves the dissipative terms given by the multi-relaxation-time scheme [17]. In addition, it realizes the expansion of the Maxwell-Jüttner distribution on a cubic lattice, in contrast to Ref. [13]. We can also construct a relativistic lattice Boltzmann model that recovers only up to second order (the momentum-energy tensor), to compare with the third-order model and determine the influence of the third-order moment in the expansion. Details of the second-order model can be found in Appendix A.

III. NUMERICAL VALIDATION

In order to validate our model, we solve the Riemann problem for a quark-gluon plasma and compare the results with BAMPS and two previous relativistic Boltzmann models. The first one, proposed by Mendoza *et al.* [7,8] and later improved by Hupp *et al.* [10], we will denote simply by RLB; and the second one, which is a recent extension of RLB developed by Li *et al.* [17] to include multi-relaxation-time, we will denote by MRT RLB. BAMPS was developed by Xu and Greiner [11] and applied to the Riemann problem in quark-gluon plasma by Bouras *et al.* [12]. Since BAMPS solves the full relativistic Boltzmann equation, we take its result as a reference to access the accuracy of our model. However, we keep in mind that BAMPS also produces approximate solutions. The present model is hereafter denoted by RLBD (RLB with dissipation).

For small ratios η/s, where s is the entropy density, RLB and MRT RLB reproduced BAMPS results to a satisfactory degree of accuracy. However, for higher $\eta/s \geq 0.1$ and moderately fast fluids, $\gamma \sim 1.3$, RLB failed to reproduce the velocity and pressure profiles [10]. MRT RLB yielded good agreement with the results at $\eta/s = 0.1$, but presented notable discrepancies for $\eta/s = 0.5$. The failure of both RLB and MRT RLB to solve the Riemann problem for high-viscosity fluids can be ascribed to their inability to recover the third-order moment of the distribution [10,17].

In this section, we will study the case of high $\eta/s \geq 0.1$ in a regime of moderate velocities. We perform the simulations on a lattice with $1 \times 1 \times 1600$ cells, only half of which are represented in our domain owing to symmetry conditions (the other half is a mirror, in order to use periodic boundary conditions for simplicity). Therefore, our simulation consists of $1 \times 1 \times 800$ lattice sites, with $\delta x = 0.008$ fm and $\delta t = \sqrt{410}.008$ fm/c for RLBD third order, and $\delta t = 0.024$ fm/c for RLBD second order.

The initial conditions for the pressure are $P_0 = 5.43$ GeV/fm^3 and $P_1 = 0.339$ GeV/fm^3. In numerical units, they correspond to 1.0 and 0.062, respectively. The initial temperature $z \geq 0$ is $T_1 = 200$ MeV (in numerical units 0.5), and $T_0 = 400$ MeV for $z < 0$, which corresponds to 1.0 in numerical units. The entropy density s is calculated according to the relation $s = 4n - n\ln(n/n^{\mathrm{eq}})$, where n^{eq} is the density calculated with the equilibrium distribution, $n^{\mathrm{eq}} = d_G T^3/\pi^2$, with $d_G = 16$ being the degeneracy of the gluons.

The velocity and pressure profiles at $t = 3.2$ fm/c with viscosity-entropy density ratios of $\eta/s = 0.1$ are shown in Fig. 2. In this figure, we compare the results with BAMPS and RLB, where we can see that RLB presents a discontinuity at $z = 0$, while both second-order and third-order RLBD get closer to the BAMPS solution. Since the only difference between second- and third-order RLBD is the third-order moment of the distribution, we conclude that at

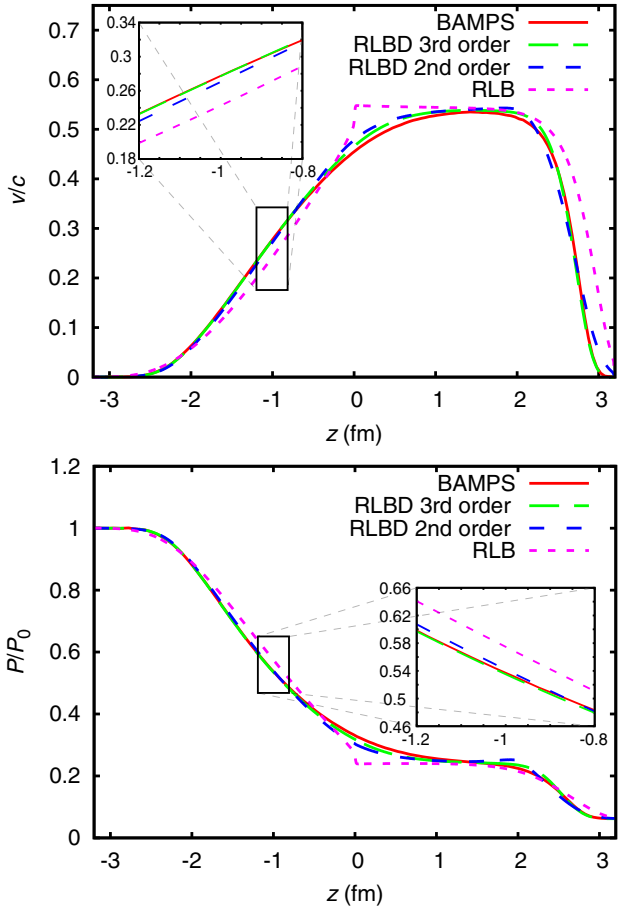

FIG. 2 (color online). Velocity (top) and pressure (bottom) profiles as functions of the z coordinate for the case of a shock wave in quark-gluon plasma, with $\eta/s = 0.1$.

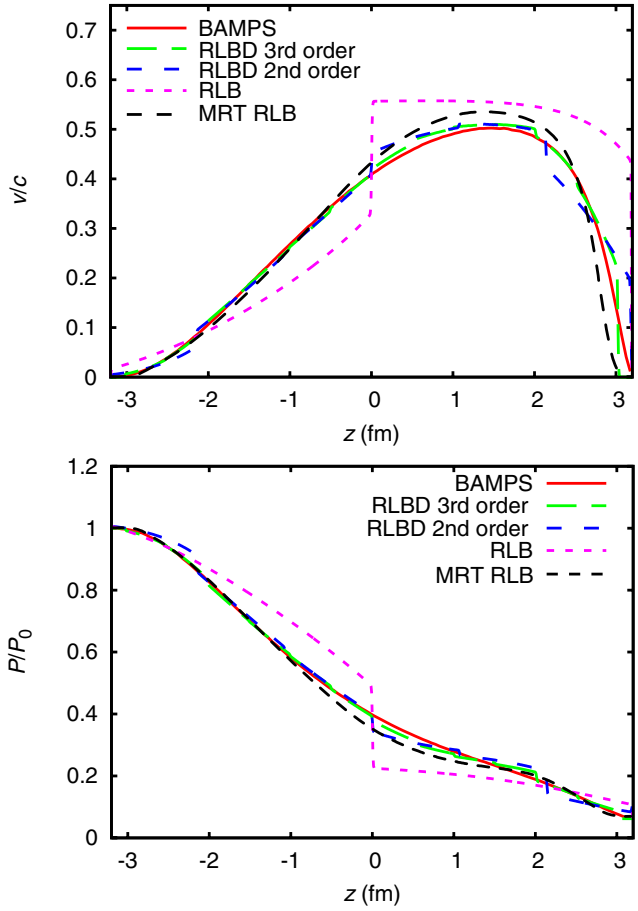

FIG. 3 (color online). Velocity (top) and pressure (bottom) profiles as functions of the z coordinate for the case of a shock wave in quark-gluon plasma, with $\eta/s = 0.5$.

relatively low η/s, the third order does not play a crucial role in either the conservative dynamics or the dissipative dynamics of the system. However, note that at $z \sim 3$ fm, the third-order model provides an outstanding fit of the numerical results by BAMPS.

On the other hand, by increasing the ratio η/s, we see from Fig. 3 that, while RLB gets worse and the second-order RLBD fixes the discrepancy only in part, the third-order RLBD improves significantly the accuracy of the velocity and pressure profiles.

In Fig. 3, we also compare the results obtained with MRT RLB and BAMPS, for $\eta/s = 0.5$. Here, a significant improvement is again appreciated, including the attainment of the right value of the maximum velocity (at $z \sim 1.5$ fm). In the pressure profile, RLBD gets closer to BAMPS than MRT RLB in the region of the discontinuity in the initial condition ($z \sim 0$).

Note that there is a staircase shape in the results of RLBD for $\eta/s = 0.5$ in Fig. 3. This is due to the large values taken by the single relaxation time in order to achieve such shear viscosity-entropy density ratios, $\tau \sim 20$–40 (in numerical units), which is beyond the hydrodynamic approximation.

As a result, higher-order moments (fourth and higher orders) of the distribution function would be required, which is not fulfilled in our RLBD model. In order to prove this statement, we have performed separate simulations (see Fig. 4), where we observe that by increasing the value of the reference temperature of the lattice (typically set at $T = 1$), so as to achieve the same shear viscosity, $\eta = (2/3)nT(\tau - 1/2)/R$, the value of τ decreases and the staircase disappears. In particular, for $T \geq 2.5$, the results come closer to the ones with BAMPS, and become independent of the reference temperature. However, due to the discretization procedure used to develop this model, whenever the reference temperature $T > 4$, the model becomes unstable, most likely because in such a parameter range, the expanded equilibrium distribution function is no longer positive definite.

We can also study the viscous pressure tensor and the heat flux for both cases, $\eta/s = 0.1$ and 0.5, which gives more insights on the dissipative properties of the model. In the Landau-Lifshitz decomposition, the viscous pressure tensor, $\pi^{\alpha\beta}$, can be calculated directly from the distribution function as

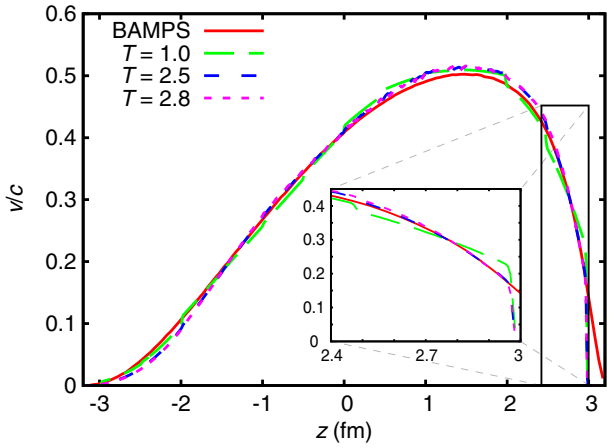

FIG. 4 (color online). Velocity profile as a function of the z coordinate for the case of a shock wave in quark-gluon plasma, with $\eta/s = 0.5$; increasing the reference numerical temperature in the lattice leads to a smaller relaxation time τ.

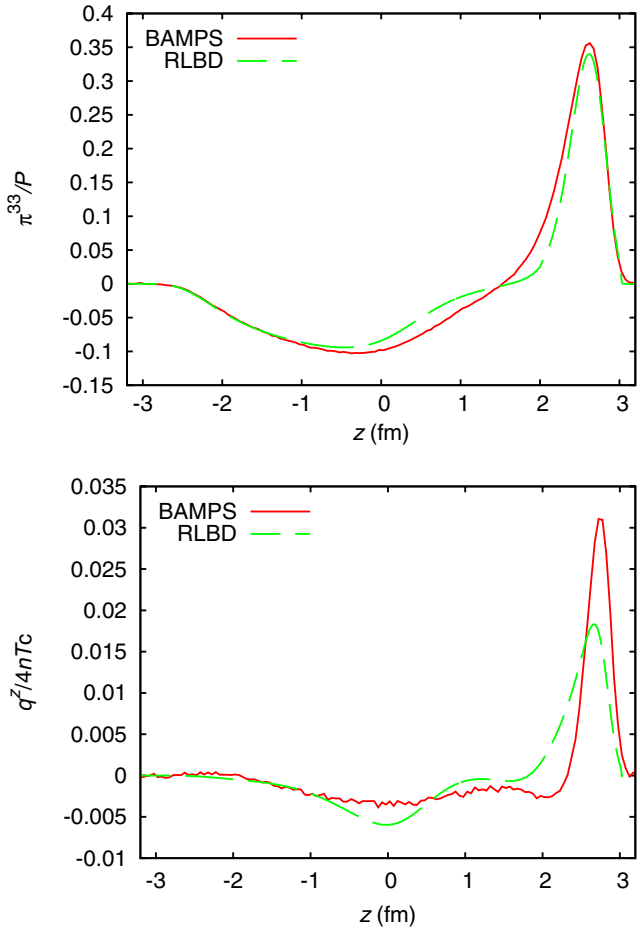

FIG. 5 (color online). Viscous pressure tensor (top) and heat flux (bottom) profiles as functions of the z coordinate for the case of a shock wave in quark-gluon plasma, with $\eta/s = 0.1$. Here, RLBD denotes the present third-order model.

$$\pi^{\alpha\beta} = \sum_{i=1}^{128} (f_i - f_i^{\mathrm{eq}}) p_i^\alpha p_i^\beta, \tag{44}$$

and the heat flux with the relation

$$q^\alpha = 4T(nU^\alpha - N^\alpha). \tag{45}$$

Note that according to Eq. (43), we have $q^\alpha U_\alpha = 0$. In Figs. 5 and 6, we observe that the component π^{33} presents good agreement with the results from BAMPS, but the heat flux exhibits a larger deviation. The reason for this discrepancy is as follows: We are fixing the value of η/s; i.e., we calculate τ locally and at each time step, such that η/s remains constant. Therefore, even if the simulations take place at the same shear viscosity, they are not, in general, for the same thermal conductivity, thereby providing different results for the heat flux. Furthermore, since the present single-relaxation-time model has only one relaxation time τ, we cannot fix the shear viscosity and the thermal conductivity independently. On the other hand, the small differences in the viscous pressure tensor between RLBD and BAMPS are most likely due to the fact that we are not reproducing correctly the fourth- and fifth-order moments of the equilibrium distribution.

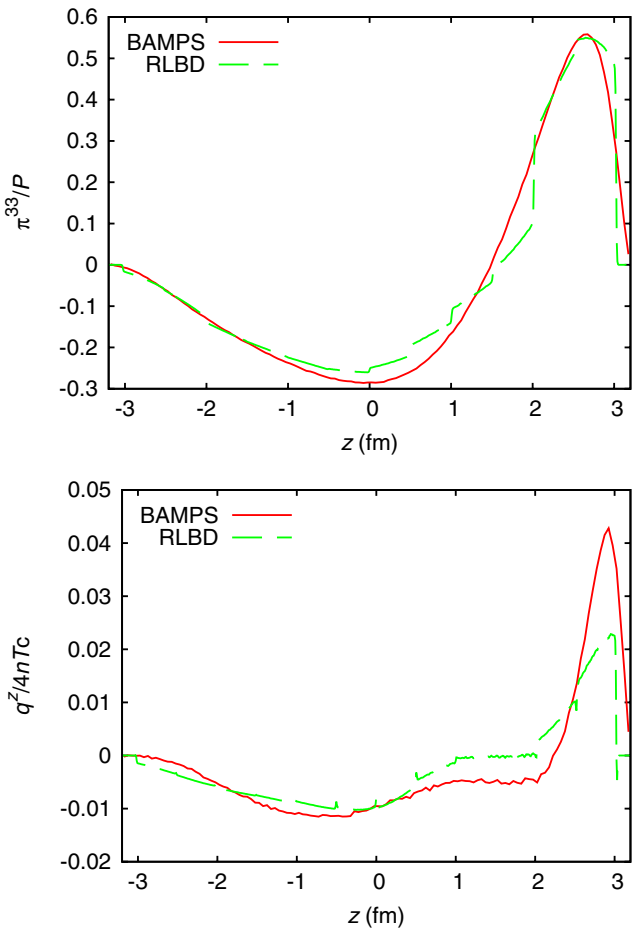

FIG. 6 (color online). The same as Fig. 5, for $\eta/s = 0.5$.

IV. CONCLUSIONS AND DISCUSSIONS

We have introduced a new relativistic lattice Boltzmann model with improved dissipation, as compared to RLB and MRT RLB. To this purpose, we have performed an expansion of the Maxwell-Jüttner distribution onto an orthonormal basis of polynomials in the 4-momentum space. In addition, in order to make the model compatible with a regular cubic lattice, we have performed the expansion in Cartesian coordinates and applied a time transformation, such that particles travel just the distance necessary to reach lattice nodes, always at the speed of light. The time transformation generates a sphere of radius R which intersects the cubic lattice, the intersection points being lattice nodes by construction. In addition, we have reproduced up to second-order moments of the equilibrium distribution, and up to third-order moments, finding $R = 3$ and $R = \sqrt{41}$ for second- and third-order moment compatibility, respectively.

The discrete energy component of the 4-momentum, p^0, has been calculated by using Gaussian quadrature, the nodes corresponding to the zeros of the next-order polynomial. With this configuration, we need 90 vectors for recovering second order and 384 for the third-order moment case. However, only 66 and 128, respectively, are actually needed to calculate the moments correctly.

In order to validate the model, we have compared our results with BAMPS, as well as previous RLB models. We have found that for $\eta/s = 0.1$, our model accurately describes the Riemann problem in quark-gluon plasma, including the expansion up to second order. However, for the case of $\eta/s = 0.5$, the second-order model, although better than RLB, is less accurate than both MRT RLB and the third-order model. The third-order model yields better results than the previous RLB, but it develops a staircase shape as a consequence of the large value of the single relaxation time, which lies beyond the hydrodynamic regime. We have shown that the staircase pathology can be tamed by increasing the reference temperature in the model. Nevertheless, increasing the reference temperature beyond $T = 4$ hits against stability limits of the model. Furthermore, we have also compared the viscous pressure tensor, $\pi^{\alpha\beta}$, and the heat flux, q^{α}, for both simulations, RLBD and BAMPS, finding good agreement for the case of $\pi^{\alpha\beta}$ but not so good for q^{α}. This is because our model has one relaxation time, and we cannot set the shear viscosity and the thermal conductivity simultaneously for the same simulation. However, our model is several orders of magnitude faster than models based on the full Boltzmann equation, and 1 order of magnitude faster than hydrocodes.

We may envisage that a multi-relaxation-time extension of the present model would further improve the accuracy of the results. A similar improvement may be anticipated by implementing higher-order expansions of the equilibrium distribution. However, since the transport coefficients depend on the collision operator, their calculation within a multi-relaxation-time model becomes increasingly involved. On the other hand, by performing expansions to include higher-order moments, the value of R might become unpractically large, with several ensuing discretization issues. Notwithstanding such potential difficulties, these extensions are surely worth being analyzed in depth for the future.

ACKNOWLEDGMENTS

We acknowledge financial support from European Research Council (ERC) Advanced Grant No. 319968-FlowCCS. The work of I. K. was supported by ERC Advanced Grant No. 291094-ELBM. The authors also wish to thank Ioannis Bouras for providing the numerical data from BAMPS simulations.

APPENDIX A: SECOND-ORDER RELATIVISTIC LATTICE BOLTZMANN MODEL

To construct the second-order lattice Boltzmann model, we use the procedure described in this paper. We have obtained that $R = 3$ presents enough symmetries to fulfill the conditions in Eq. (25), and the velocity vectors $\vec{\vartheta}$ are given by $(\pm 3, 0, 0)$, $(0, \pm 3, 0)$, $(0, 0, \pm 3)$, $(\pm 2, \pm 1, \pm 2)$, $(\pm 1, \pm 2, \pm 2)$, and $(\pm 2, \pm 2, \pm 1)$. The values for the discrete p^0 come from the solution of the equation

$$\mathcal{R}^{(3)} = \frac{1}{12} p^0 (p^0 - 6)^2 - 2 = 0, \tag{A1}$$

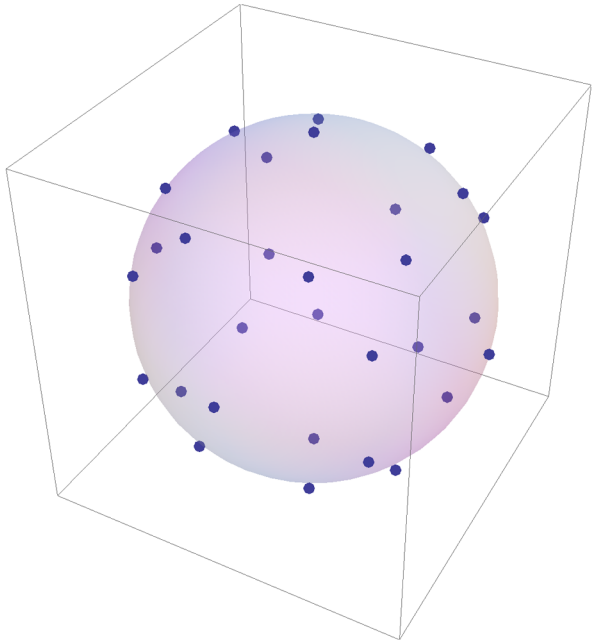

FIG. 7 (color online). Directions of the velocity vectors $\vec{\vartheta}_i$ to recover up to the second-order moment of the Maxwell-Jüttner distribution, namely the momentum-energy tensor. The radius of the sphere is $R = 3$. The points represent lattice sites belonging to the surface of the sphere.

instead of $\mathcal{R}^{(4)}$ for the case of the third-order expansion. This gives the values $p_l^0 \simeq 0.936$, 3.305, and 7.759. The discrete 4-momentum vectors p_i^μ are constructed with Eqs. (20) and (24), and they are, in total, $\mathcal{N} = 3 \times 30 = 90$. However, as in the third-order expansion, we have retained the minimal number out of 90 that are necessary to recover the second-order moment, by imposing the maximum number of w_i to be zero. This gives only 66 4-momentum vectors. The value of the weight functions for every momentum vector and the relations with the 30 directions are given in the Supplemental Material [21]. In Fig. 7, we report the spatial configuration of the vectors $\vec{\vartheta}_i$.

The discrete version of the relativistic Boltzmann equation, Eq. (40), still applies, and the discrete equilibrium distribution function is written in detail in Eq. (B1) of Appendix B. However, due to the fact that the third-order moment is not satisfied, an analytical theory to calculate the transport coefficients would be very complicated and goes beyond the scope of this work. Therefore, we have calculated numerically only the shear viscosity, by matching the results for low velocity with the third-order moment model, in order to compare the results of both expansions with other models in the literature. This gives a shear viscosity $\eta_{2\mathrm{nd}} \sim (1/7)P(\tau - \delta t/2)/R$. We could, in principle, calculate the third-order moment associated with the equilibrium distribution given by Eq. (B1) and, by applying the Grad method, compute the other transport coefficients. However, this procedure would need to be performed entirely numerically, since the weights w_i and 4-momentum vectors p_i^μ are only known numerically. Since the main purpose of this paper is to improve the description of dissipative effects by performing the third-order expansion and placing it on a cubic lattice, we are not interested in the bulk viscosity and the thermal conductivity for this case, and leave this task for future work.

APPENDIX B: EQUILIBRIUM DISTRIBUTION FUNCTIONS

The equilibrium distribution function capable of recovering the first- and second-order moments of the equilibrium distribution is calculated by using up to the second order polynomials in Eq. (12), namely the 14 polynomials J_k with $k = 0, \ldots, 13$, obtaining

$$
\begin{aligned}
f_i^{\mathrm{eq}} = \frac{nw_i}{4T}[&p_i^{02}(T^2(2U^{02} - U^{x2} - U^{y2} - 1) - 2TU^0 + 1) + 2p_i^0(T(T(U^0(p_i^x U^x + p_i^y U^y + p_i^z U^z - 4U^0) + 1) \\
&- p_i^x U^x - p_i^y U^y - p_i^z U^z + 7U^0) - 4) + T^2(p_i^{x2}(-U^{02} + 2U^{x2} + U^{y2} + 1) \\
&+ 2p_i^x U^x(p_i^y U^y + p_i^z U^z - 4U^0) + p_i^{y2}(-U^{02} + U^{x2} + 2U^{y2} + 1) + 2p_i^y U^y(p_i^z U^z - 4U^0) \\
&+ 8U^0(U^0 - p_i^z U^z) - 2) + 2T(5(p_i^x U^x + p_i^y U^y + p_i^z U^z) - 8U^0) + 12].
\end{aligned} \tag{B1}
$$

For the case of the third-order moment expansion, we repeat the same procedure, using all the polynomials ($k = 0, \ldots, 29$). This leads to the following expressions:

$$
\begin{aligned}
f_i^{\mathrm{eq}} = \frac{nw_i}{12T}[&p_i^{03}(TU^0 - 1)(T^2(4U^{02} - 3(U^{x2} + U^{y2} + 1)) - 2TU^0 + 1) \\
&- p_i^{02}(T^3(-2U^{02}(3p_i^x U^x + 3p_i^y U^y + 2p_i^z U^z) + (U^{x2} + U^{y2} + 1)(3p_i^x U^x + 3p_i^y U^y + p_i^z U^z) \\
&+ 36U^{03} - 6U^0(3U^{x2} + 3U^{y2} + 4)) + 3T^2(2U^0(p_i^x U^x + p_i^y U^y + p_i^z U^z) - 22U^{02} + 7(U^{x2} + U^{y2}) + 9) \\
&- 3T(p_i^x U^x + p_i^y U^y + p_i^z U^z - 14U^0) - 15) - 3p_i^0(T^3(U^{03}(p_i^{x2} + p_i^{y2} - 24) - U^0(p_i^{x2}(2U^{x2} + U^{y2} + 1) \\
&+ 2p_i^x U^x(p_i^y U^y + p_i^z U^z) + p_i^y(p_i^y U^{x2} + 2p_i^y U^{y2} + p_i^y + 2p_i^z U^y U^z) - 12) + 12U^{02}(p_i^x U^x + p_i^y U^y + p_i^z U^z) \\
&- 2(p_i^x U^x + p_i^y U^y + p_i^z U^z)) + T^2(p_i^{x2}(-U^{02} + 2U^{x2} + U^{y2} + 1) + 2p_i^x U^x(p_i^y U^y + p_i^z U^z - 11U^0) \\
&+ p_i^{y2}(-U^{02} + U^{x2} + 2U^{y2} + 1) + 2p_i^y U^y(p_i^z U^z - 11U^0) - 22p_i^z U^0 U^z + 56U^{02} - 14) \\
&+ 2T(6(p_i^x U^x + p_i^y U^y + p_i^z U^z) - 25U^0) + 20) + T(p_i^{x3} T^2 U^x(-3U^{02} + 4U^{x2} + 3U^{y2} + 3) \\
&+ p_i^{x2} T(3(U^{02} - 2U^{x2} - U^{y2} - 1)(-p_i^y TU^y + 6TU^0 - 7) + p_i^z TU^z(-U^{02} + 4U^{x2} + U^{y2} + 1)) \\
&+ 3p_i^x U^x(T(T(p_i^{y2}(-U^{02} + U^{x2} + 2U^{y2} + 1) + 2p_i^y U^y(p_i^z U^z - 6U^0) - 12p_i^z U^0 U^z + 24U^{02} - 4) \\
&+ 14p_i^y U^y + 14p_i^z U^z - 48U^0) + 30) + p_i^{y3} T^2 U^y(-3U^{02} + 3U^{x2} + 4U^{y2} + 3) \\
&+ p_i^{y2} T(p_i^z TU^z(-U^{02} + U^{x2} + 4U^{y2} + 1) + 3(6TU^0 - 7)(U^{02} - U^{x2} - 2U^{y2} - 1)) \\
&+ 6p_i^y U^y(T(2T(-3p_i^z U^0 U^z + 6U^{02} - 1) + 7p_i^z U^z - 24U^0) + 15) + 6p_i^z U^z(2T^2(6U^{02} - 1) - 24TU^0 + 15) \\
&- 24U^0(T^2(2U^{02} - 1) - 5TU^0 + 5)) - 30(T^2 - 2)].
\end{aligned} \tag{B2}
$$

[1] K. S. Novoselov, A. K. Geim, S. V. Morozov, D. Jiang, Y. Zhang, S. V. Dubonos, I. V. Grigorieva, and A. A. Firsov, Science **306**, 666 (2004).
[2] K. S. Novoselov, A. K. Geim, S. V. Morozov, D. Jiang, M. I. Katsnelson, I. V. Grigorieva, S. V. Dubonos, and A. A. Firsov, Nature (London) **438**, 197 (2005).
[3] M. Müller, J. Schmalian, and L. Fritz, Phys. Rev. Lett. **103**, 025301 (2009).
[4] E. Shuryak, Prog. Part. Nucl. Phys. **53**, 273 (2004).
[5] P. K. Kovtun, D. T. Son, and A. O. Starinets, Phys. Rev. Lett. **94**, 111601 (2005).
[6] G. Policastro, D. T. Son, and A. O. Starinets, Phys. Rev. Lett. **87**, 081601 (2001).
[7] M. Mendoza, B. M. Boghosian, H. J. Herrmann, and S. Succi, Phys. Rev. Lett. **105**, 014502 (2010).
[8] M. Mendoza, B. M. Boghosian, H. J. Herrmann, and S. Succi, Phys. Rev. D **82**, 105008 (2010).
[9] R. Benzi, S. Succi, and Vergassola, Phys. Rep. **222**, 145 (1992).
[10] D. Hupp, M. Mendoza, I. Bouras, S. Succi, and H. J. Herrmann, Phys. Rev. D **84**, 125015 (2011).
[11] Z. Xu and C. Greiner, Phys. Rev. C **71**, 064901 (2005).
[12] I. Bouras, E. Molnar, H. Niemi, Z. Xu, A. El, O. Fochler, C. Greiner, and D. H. Rischke, Phys. Rev. Lett. **103**, 032301 (2009).
[13] P. Romatschke, M. Mendoza, and S. Succi, Phys. Rev. C **84**, 034903 (2011).
[14] C. Cercignani and G. M. Kremer, *The Relativistic Boltzmann Equation: Theory and Applications* (Birkhauser, Basel, 2002).
[15] X. He and L.-S. Luo, Phys. Rev. E **56**, 6811 (1997).
[16] N. S. Martys, X. Shan, and H. Chen, Phys. Rev. E **58**, 6855 (1998).
[17] Q. Li, K. H. Luo, and X. J. Li, Phys. Rev. D **86**, 085044 (2012).
[18] S. S. Chikatamarla and I. V. Karlin, Phys. Rev. Lett. **97**, 090601 (2006).
[19] S. S. Chikatamarla and I. V. Karlin, Phys. Rev. E **79**, 046701 (2009).
[20] J. Anderson and H. Witting, Physica (Utrecht) **74**, 466 (1974).
[21] See Supplemental Material at http://link.aps.org/supplemental/10.1103/PhysRevD.87.065027 for detailed information about the numerical values of the discrete 4-momentum vectors and weighting functions needed to recover the second and third order moments of the equilibrium distribution.